CORROSION SCIENCE AND TECHNOLOGY, Vol.16, No.3(2017), pp.109~114 pISSN: 1598-6462 / eISSN: 2288-6524
[Research Paper] DOI: https://doi.org/10.14773/cst.2017.16.3.109

Monitoring Cathodic Shielding and Corrosion under Disbonded Coatings

F. Varela, M. YJ Tan†, B. Hinton, and M. Forsyth
Institute for Frontier Materials, Deakin University, Victoria 3220, Australia
(Received June 03, 2017; Revised June 12, 2017; Accepted June 13, 2017)

Monitoring of corrosion is in most cases based on simulation of environmental conditions on a large and complex structure such as a buried pipeline using a small probe, and the measurement of thermodynamics and kinetics of corrosion processes occurring on the probe surface. This paper presents a hybrid corrosion monitoring probe designed for simulating deteriorating conditions wrought by disbonded coatings and for measuring current densities and distribution of such densities on a simulated pipeline surface. The concept of the probe was experimentally evaluated using immersion tests under cathodic protection (CP) in high resistivity aqueous solution. Underneath the disbonded area, anodic currents and cathodic currents were carefully measured. Anodic current densities were used to calculate metal loss according to Faraday's law. Calculated corrosion patterns were compared with corrosion damage observed at the surface of the probe after a series of stringent tests. The capability of the probe to measure anodic current densities under CP, without requiring interruption, was demonstrated in high resistivity aqueous solution. The pattern of calculated metal loss correlated well with corrosion products distribution observed at the array surface. Working principles of the probe are explained in terms of electrochemistry.

Keywords: *pipeline, steel, cathodic protection, corrosion monitoring, aqueous solution, electrochemistry*

1. Introduction

Corrosion monitoring is often based on the simulation of environmental conditions on a large and complex structure such as a buried pipeline using a small probe, and the measurement of the thermodynamics and kinetics of corrosion processes occurring on the probe surface. If corrosion processes are properly simulated, the probe can provide useful information on corrosion over the larger structure. This concept has been successfully implemented in many industries such as the petrochemical industry. However, corrosion monitoring of underground pipelines remains a challenge. In the highly resistive soil environment, the use of impressed current cathodic protection (CP) systems and the presence of barrier coatings make corrosion monitoring difficult. For instance, CP introduces a great complication to traditional electrochemical corrosion monitoring techniques because they are only applicable around the open circuit potential [1-3]. The application of non-electrochemical techniques such as corrosion coupons can also be difficult for underground applications because of the need for costly underground installation/extractions. Corrosion coupons would only be able to provide time averaged information after a long exposure to the environment. Electrical resistance probes can provide in-situ data, however in principle they are unable to measure localised corrosion because localised damages such as pitting may not lead to any significant change in electric resistance. Unfortunately localised forms of corrosion are often the type of attack found in pipelines.

On the other hand, the use of barrier coatings on pipelines introduces some other complexities for corrosion monitoring. For instance a common form of pipeline damage is related to coating disbondment that generates a crevice between the disbonded coating film and the metallic pipe. This type of coating defect requires particular attention since it is found to be related to the most severe localised corrosion issues in pipelines [4-7]. It is known from published modelling and experimental works that the environment under disbonded coatings deviates significantly from the bulk. Due to the shielding of CP currents and isolation of the external environment, the crevice area develops a complex environment with high cation concentrations [8-11], high pH (in most cases) [8-10,12-17], negligible oxygen [9,10,12,15-18] and a gradient of potentials [8,9,11-22]. The initiation and propagation of localised corrosion under disbonded pipeline coatings are

† Corresponding author: mike.tan@deakin.edu.au

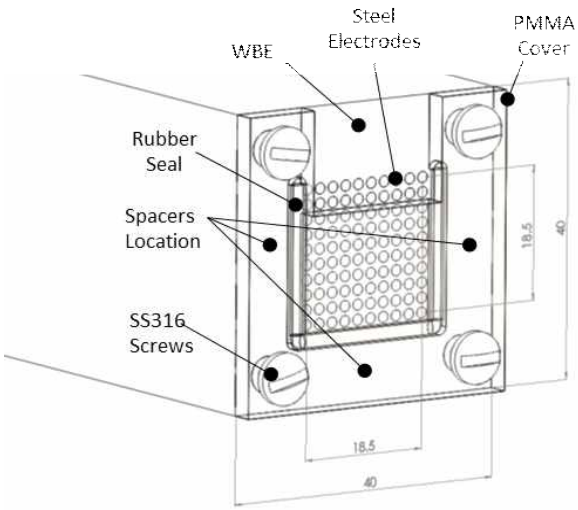

Fig. 1 New probe's assembly.

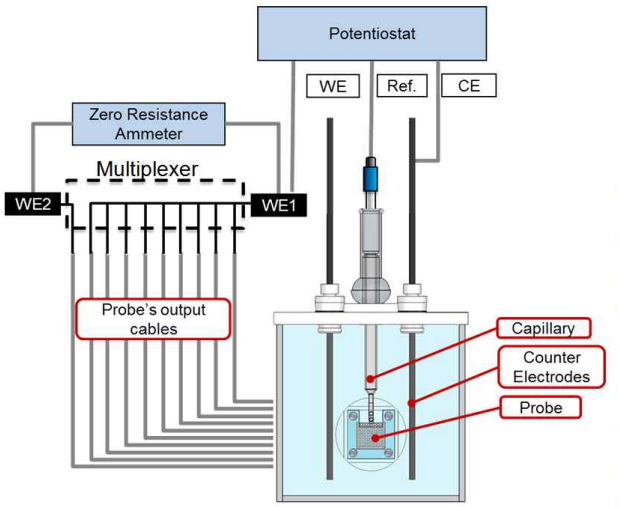

Fig. 2 A schematic diagram of the experimental setup.

considered to be extremely challenging to monitor; at present there is no sensor technology that possesses the abilities of providing in-situ information regarding them [19].

The purpose of this paper is to develop a new CP compatible localised corrosion monitoring method for the pipeline industry. The most important component of the method is a novel corrosion monitoring probe that is capable of simulating the evolution of the environment under disbonded coatings and measure the initiation and propagation of localised corrosion under disbonded pipeline coatings under CP.

2. Method and Experimental Procedure

As shown in Fig. 1, a novel corrosion monitoring probe was designed for simulating and evaluating current density profiles along a simulated coating disbondment area. The probe's design is based on an interconnected electrode array. Closely packed electrode arrays allow the simulation of a metallic surface while independent electrochemical measurements between wires can be performed [23,24]. This design allows proper simulation of the gradients of pH, nonuniform oxygen distribution and lack of CP effectiveness by exposing the array to inhomogeneous conditions under a simulated disbonded coating layer.

3. Experimental Setup

For the proof of concept, a probe was made based on a Wire Beam Electrode (WBE) consisting of a one hundred 1.59mm diameter UNS no. G0350 wires mounted in epoxy in a 10 by 10 array of 18.5 by 18.5mm. Fig. 1 presents a schematic view of this electrode array and the rest of the probe assembly. To simulate a perfectly CP shielding disbonded coating, a polymethyl methacrylate (PMMA) cover was used. The cover did not shield the whole array; instead the first two rows of electrodes were left to simulate a coating defect. A rubber seal was used to prevent the solution ingress around the edges of the electrode array. This seal was held in place by a groove machined in the PMMA cover. The array surface was abraded to 1200 grit using silicon carbide paper and using water as lubricant. After abrading, the array was immediately rinsed with ethanol and acetone. The simulated disbonded coating was then installed on top of the array using four stainless steel 316 screws. To achieve an even crevice gap of 0.25 mm, cellophane film fragments were used as spacers by placing them in the locations indicated in Fig. 1. A schematic representation of the experimental setup used is presented in Fig. 2. The probe was installed in a 2.5 L electrochemical cell.

The probe was connected to a programmable multiplexer and measuring instrument using computer cables. To measure the net current values at each electrode, a Zero Resistance Ammeter (ZRA) was interconnected between WE1 and WE2. At any time 99 electrodes were connected to WE1 and the remaining electrode was connected to the WE2 (see Fig. 2). All potentials were measured against a Ag/AgCl/Sat. KCl reference electrode (Ref.). The ZRA allowed to achieve the same electrical potential between WE1 and WE2, maintaining all electrodes constantly under CP. CP was applied by fixing the probe's potential at –760 $mV_{Ag/AgCl}$ (-850 mV_{CSE}), using a potentiostat in a traditional three electrodes configuration where WE1 was used as working electrode (WE).

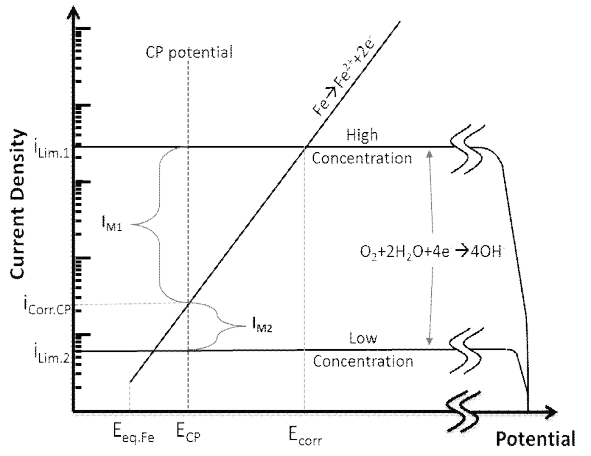

Fig. 3 A schematic Evan's diagram of the probe's working principle.

Counter Electrodes (CE) consisted of two Ø4.5 mm graphite rods of 120 mm long were immersed in the test solution to provide CP to the system. To minimize IR drops, a Luggin capillary was used.

A test solution representative of highly resistive soils was used in this test. The 5000 ohm·cm, 0.001 M Na_2SO_4 test solution was prepared from analytical grade reagents and ASTM D1193 ultrapure water [25]. Air was purged through the solution for at least 2 h before the test to ensure an initial oxygen saturation concentration. The test was performed in an open to air condition. During the test, current scans were performed every 20 min for the 23 h immersion period. Tests were performed in duplicates at room temperature (22 ºC).

A post processing script for MATLAB was used to analyse the local current data recorded by the ZRA. This script constructed current density distribution maps based on the ZRA data, the multiplexer scanning sequence and the electrodes addresses. Current densities were calculated based on the area of a single electrode (1.98 mm^2). An Evan's diagram, as shown in Fig. 3, was used to aid the interpretation of the current distribution maps. A metal losses map was also calculated by applying Faraday's law to the accumulated charge of the anodic currents registered by the probe.

4. Results and Disscusion

Fig. 4 presents the current density distribution maps obtained by the probe at different immersion times over a 22 h test period. Anodic current densities are represented by positive values while cathodics are represented by negatives values. The first two rows of each current density map corresponds to the uncovered electrodes area (simulating coating defect areas), while the rest show the behaviour within the area under the crevice (simulating disbonded coating areas).

In general, large cathodic current densities were found at the uncovered electrode areas. Anodic current densities were only detected under the disbonded area and the value decreased as the test progressed. The CP current profiles obtained with the probe (see Fig. 4) correlate well with the results presented in other published works where significantly larger cathodic current densities were reported at the crevice opening [11,18,20,26,27]. However, anodic current densities were rarely reported before, they were detected occasionally as insolates data points and were often disregarded [26,27]. Particularly, Li et al. [20] reported anodic current densities at an electrode being preferentially corroded under a simulated disbonded coating, but no explanation regarding how their segmented electrode was capable of detecting anodic currents under CP was presented.

A key concept needed to understand the probe's working principle is that the current registered by each electrode of the array is net current resulting from all anodic and cathodic processes occurring at its surface. Consequently, the factors affecting this process along the crevice and uncovered areas have a marked effect on the currents registered. It has been previously reported in the literature that parameters such as potential [8,9,11-22], pH [8-10, 12-17], oxygen concentration [9,10,12,15-18] and concentration of other species [8-11] change considerably along disbonded areas. At the CP potential evaluated in this work (it is the minimum protection potential accepted by pipeline industry), dissolved oxygen concentration is the main factor affecting the cathodic reactions rate.

A schematic Evan's diagram showing the effect of oxygen depletion on the currents measured by the array is presented in Fig. 3. The larger oxygen reduction limiting current case ($i_{Lim.1}$) represents the conditions at the uncovered electrodes, where the oxygen concentration is high. At this location, cathodic current densities ($i_{Lim.1}$) are larger than anodic current ($i_{corr.CP}$) and therefore, the net current densities measured by the array electrodes (I_{M1}) are cathodic despite some anodic reaction (i.e. corrosion reaction) may still take place ($i_{corr.CP} > 0$). When considering the lower oxygen reduction limiting current case ($i_{Lim.2}$) that corresponds to the nearly depleted oxygen environment in the crevice area, the anodic current densities ($i_{corr.CP}$) could be larger than cathodic currents ($i_{Lim.2}$). Consequently, the current densities measured at this location are anodic (I_{M2}) even though both locations were considered at same CP potential in this hypothetical case. In

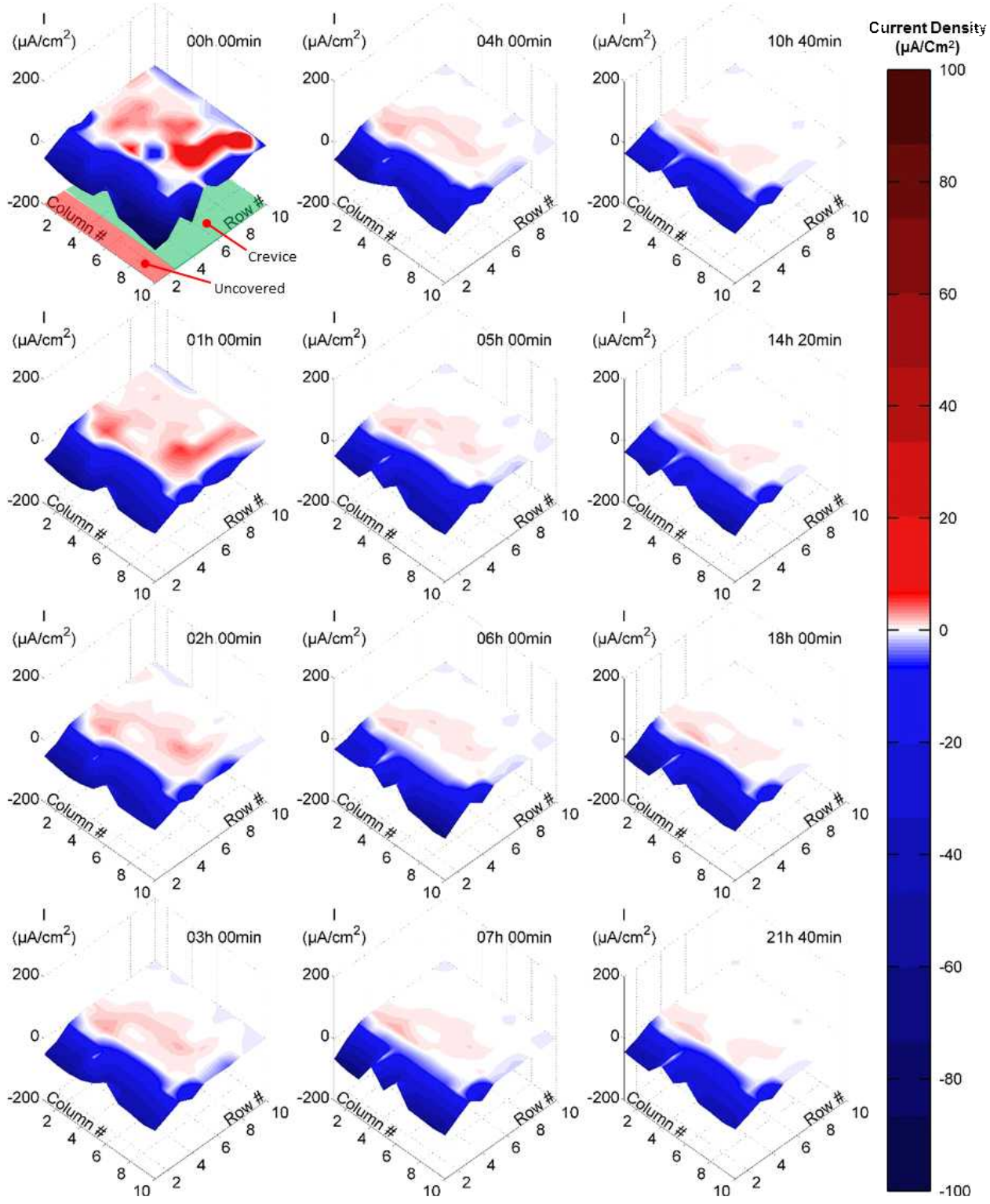

Fig. 4 Current density distribution maps at several immersion times in 0.001 M Na_2SO_4 at −760 $mV_{Ag/AgCl}$.

real systems, the local CP potential within the crevice could be less negative than at its opening. In addition, pH and other solution compositional changes may also affect the anodic reaction rate. Nevertheless, none of these

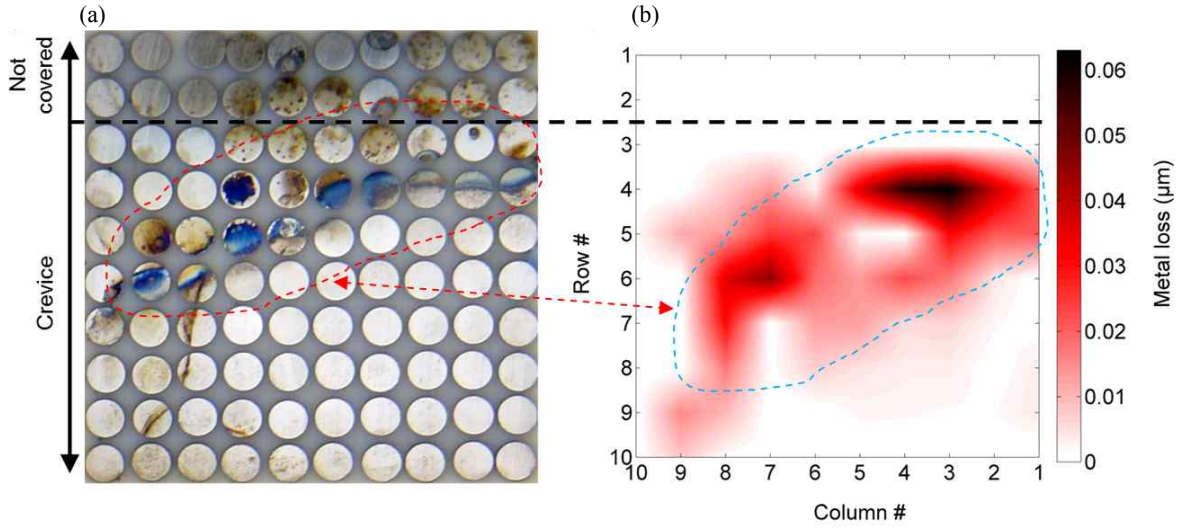

Fig. 5 Comparison between actual (a) and measured (b) corrosion patterns.

changes affect the rate of the diffusion controlled cathodic reaction, and consequently, in the absence of other cathodic reaction, the measurement of anodic current densities under the simulated disbonded coating should remain valid. We believe this discussion explains the electrode array's capability to detect anodic currents under CP under disbonded coatings.

Fig. 5 shows a comparison between the appearance of the electrode array surface at the end of the test period and the metal losses calculated form the probes data. A photograph of the electrode array is presented in Fig. 5a where corrosion can be observed mainly on areas under the simulated disbonded coating. Fig. 5b presents the metal losses calculated based on the anodic current densities detected by the probe using Faraday's law. The calculated metal losses, expressed as the thickness reduction after 23 h of exposure, shown values below 0.2 μm indicating the high sensitivity of the probe. When comparing the measured (Fig. 5b) and actual (Fig. 5a) corrosion patterns, a good correlation in the general corrosion patterns for the electrodes located within the crevice is found. However, no metal loses were detected at the top three rows of electrodes. As was explained before, the high oxygen concentration at these locations prevents the probe from measuring anodic current densities at these locations. A more advanced data analysis technique capable of estimating corrosion from the cathodic current densities measured by the array at this location is being developed to overcome this limitation and will be published elsewhere.

5. Conclusions

A new probe has been designed to perform electrochemical measurements of corrosion rates, as well as CP effectiveness, under cathodically protected disbonded coatings in highly resistive media. The probe's capability to measure anodic current densities under CP, without requiring its interruption, was demonstrated in high resistivity aqueous solution. The pattern of calculated metal losses correlated well with the corrosion products distribution observed at the array surface.

Acknowledgments

This work was funded by the Energy Pipelines CRC, supported through the Australian Government's Cooperative Research Centres Program. The funding and in-kind support from the APIA RSC is gratefully acknowledged.

References

1. J. Jankowski, *Corros. Rev.*, **20**, 159 (2002).
2. J. Jankowski, *Corros. Rev.*, **20**, 179 (2002).
3. V. Facundo, T. Y. Jun, and F. Maria, *Proc. 53th Annual Conference of the Australasian Corrosion Association*, Hinton Bruce and Bonar Craig, Brisbane, Australia (2013).
4. S. A. Shipilov and Le May I, *Eng. Fail. Anal.*, **13**, 1159 (2006).
5. S. S. Abedi, *Eng. Fail. Anal.*, **14**, 250 (2007).
6. F. Hasan, J. Iqbal, and F. Ahmed, *Eng. Fail. Anal.*, **14**, 801 (2007).
7. C. Manfredi and J. L. Otegui, *Eng. Fail. Anal.*, **9**, 495 (2002).
8. M. Yan, J. Wang, E. Han, and W. Ke, *Corros. Sci.*, **50**, 1331 (2008).
9. F. M. Song and N. Sridhar, *Corros. Sci.*, **50**, 70 (2008).
10. D. T. Chin and G. M. Sabde, *Corrosion*, **56**, 783 (2000).
11. J. Xu, C. Sun, M. Yan, and F. Wang, *Mater. Chem. Phys.*,

142, 692 (2013).
12. X. Chen, X. G. Li, C. W. Du, and Y. F. Cheng, *Corros. Sci.*, **51**, 2242 (2009).
13. A. Eslami, B. Fang, R. Kania, B. Worthingham, J. Been, R. Eadie, and W. Chen, *Corros. Sci.*, **52**, 3750 (2010).
14. A. Eslami, R. Kania, B. Worthingham, G. V. Boven, R. Eadie, and W. Chen, *Corros. Sci.*, **53**, 2318 (2011).
15. J. J. Perdomo and I. Song, *Corros. Sci.*, **42**, 1389 (2000).
16. J. J. Perdomo, M. E. Chabica, and I. Song, *Corros. Sci.*, **43**, 515 (2001).
17. F. M. Song, *Corros. Sci.*, **55**, 107 (2012).
18. D. T. Chin and G. M. Sabde, *Corrosion*, **55**, 229 (1999).
19. F. M. Song, *Corrosion*, **66**, 035005 (2010).
20. Z. Li, F. Gan, and X. Mao, *Corros. Sci.*, **44**, 689 (2002).
21. A. Eslami, R. Kania, B. Worthingham, G. V. Boven, R. Eadie, and W. Chen *Corrosion*, **69**, 1103 (2013).
22. T. R. Jack, G. V. Boven, M. Wilmott, R. L. Sutherby, and R. G. Worthingham, *Mater. Performance*, **33**, 17 (1994).
23. Y. J. Tan, *Prog. Org. Coat.*, **19**, 89 (1991).
24. Y. J. Tan and S. T. Yu, *Prog. Org. Coat.*, **19**, 257 (1991).
25. ASTM-D1193, Standard Specification for Reagent Water, ASTM International, West Conshohocken, PA (2011).
26. R. Brousseau and S. Qian, *Corrosion*, **50**, 907 (1994).
27. W. Wang, Q. Wang, C. Wang, and J. Yi, *J. Loss Prevent. Proc.*, **29**, 163 (2014).